Refractive index of thin films of SiO$_2$, ZrO$_2$, and HfO$_2$ as a function of the films' mass density

Martin Jerman, Zhaohui Qiao, and Dieter Mergel

Series of amorphous SiO$_2$, ZrO$_2$ and HfO$_2$ films were prepared by electron-beam evaporation at various oxygen pressures such that the packing density varied from 0.6 to 0.82. Transmittance spectra were evaluated with respect to thickness and refractive index by application of analytical formulas to the interference extrema and by dielectric modeling. The thickness of the films ranged from 150 to 1500 nm. The coefficients of Cauchy and Sellmeier dispersion curves were determined as a function of the packing density. The mass density of the compact amorphous grains was estimated by an effective-medium theory and a general refractivity formula. It is similar to those of the crystalline materials. We used the optical data to design multilayer coatings for laser applications in a broad spectral range, including the UV.   © 2005 Optical Society of America

OCIS codes: 310.6860, 310.6870, 310.1860, 310.3840.

1. Introduction

In the optical workshop at the University of Duisburg—Essen, customized optical coatings for laser applications are designed and produced. To design multilayer coatings according to predefined optical spectral characteristics, one has to know precise dispersion curves in the relevant spectral range of the thin-film materials involved. The films are deposited by electron-beam evaporation. For a robust production process the background pressure must not be too low, because the background pressure may change from run to run and does not yield a reproducible oxygen partial pressure. Increasing the oxygen pressure leads, however, to a decrease in the packing density of the films and to a related decrease in the refractive index, as was shown for TiO$_2$.[1] For good control of the deposition and the design of optical coatings, the packing density and the refractive index of the films as functions of the process conditions must be known.

The optical constants and the thicknesses of thin films consisting of isotropic materials can be inferred from photometric (transmittance and reflectance) measurements. In this paper, to evaluate the transmittance spectra we apply two methods: use of analytical formulas and dielectric modeling, i.e., the fit of theoretical spectra derived from physical models to experimental data. The methods are used for a variety of materials (MgF$_2$, SiO$_2$, Al$_2$O$_3$, ZrO$_2$, HfO$_2$, and TiO$_2$) with refractive indices n ranging from 1.35 to 2.5 and film thicknesses d from 150 to 1500 nm.

The relationship of the oxygen pressure during deposition, the packing density, and the refractive index of the films was investigated in more detail for SiO$_2$, HfO$_2$, and ZrO$_2$. These are hard, durable, and laser-damage-resistant materials of low (SiO$_2$) and high (HfO$_2$, ZrO$_2$) refractive index and are widely used to produce multilayered coatings, also for the UV spectral range.

2. Preparation and Characterization of the Films

The films were deposited by electron-beam evaporation of granular material (HfO$_2$, purity 99.99% excluding Zr; SiO$_2$, 99.997%; ZrO$_2$, 99.3%; Ref. 2) in a Balzers BAK-640 high-vacuum chamber pumped with a diffusion pump. The base pressure before deposition was 3×10^{-4} Pa. The oxygen pressure during deposition varied from 1 to 8×10^{-2} Pa. The deposition rate was monitored and controlled by a quartz oscillator. In every run, circular glass substrates (Schott B270; 1 mm thick, 25 mm in diameter) and quartz substrates (Schott Lithosil Q1; 2 mm thick,

The authors are with the Thin Film Technology Group, FB-7 (Department of Physics), Universität Duisburg—Essen, Campus Essen, 45117 Essen, Germany. M. Jerman (martin.jerman@uni-essen.de) is also with the Optical Workshop at the same institution.

25 mm in diameter) were mounted onto a calotte and coated while the calotte was rotating. The substrate temperature was 300 °C for most of the depositions. ZrO₂ films were also prepared at 170 °C. The thickness of the films ranged from 0.15 to 1.5 μm.

We determined the mass of the films by weighing the substrates with a comparator balance (Sartorius C50; nominal resolution, 1 μg) before and after deposition. Transmittance spectra were measured with a Perkin-Elmer Lambda-9 spectrometer. The thickness of the edge between the substrate and the film generated by the window in the substrate holder was determined by the stylus method with a Tencor T10 profilometer. The crystal structure was investigated with a Siemens Me 200 CY2 x-ray diffractometer in Bragg–Brentano geometry. No film showed crystalline peaks.

The transmittance spectra were evaluated according to the Swanepoel method described in Ref. 3. The order m of the minima of T is plotted versus $2n_m/\lambda_m$, where n_m and λ_m are the refractive indices and the positions of the minima, respectively. For SiO₂ films with refractive indices smaller than that of the B270 glass substrate, the maxima have to be taken instead. In both cases we deal with a λ/4 layer, and the formulas below are valid. The data are fitted by a straight line, and the film thickness is given as the slope of this line. Refractive index n_2 of the film at the spectral position of a minimum [or of a maximum; for conditions, see comment after Eq. (3)] is given by[4]

$$n_2 = \left(n_1 n_3 \frac{1 + \sqrt{R_c}}{1 - \sqrt{R_c}} \right)^{1/2}, \qquad (1)$$

where n_1 and n_3 are the indices of the substrate and the surrounding medium (air in our case), respectively, and R_c is the reflectance of a coated half-space. The fictitious mathematical quantity R_c is calculated from the measured transmittance of the coated and uncoated substrates, T_c and T_0, respectively[5]:

$$R_c = \frac{2T_0 - T_c(1 + T_0)}{2T_0 + T_c(T_0 - 1)}. \qquad (2)$$

Equation (1) was derived from the expression for the reflectance of a λ/4 film upon a half-infinite substrate with refractive index n_1:

$$R = \left(\frac{n_2{}^2 - n_1 n_3}{n_2{}^2 + n_1 n_3} \right)^2, \qquad (3)$$

which is valid when $n_1 > n_2 > n_3$, yielding a minimum of reflectance, and when $n_1 < n_2 > n_3$, yielding a maximum of reflectance.[5] Equations (1) and (2) together are equivalent to Eqs. (8) and (9) of Ref. 3.

Alternatively, we calculate theoretical spectra by dielectric modeling and fit them to the experimental data by varying the parameters of the model. We used a commercial software program that was al-
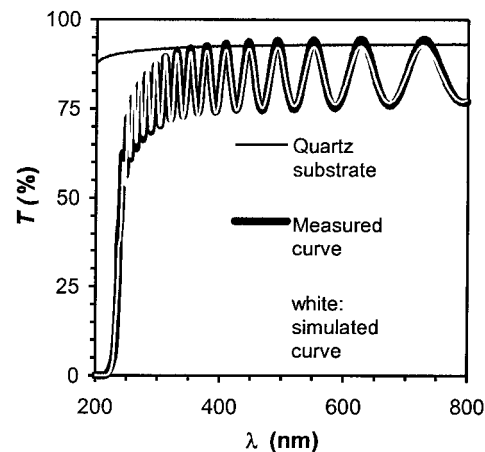

Fig. 1. Transmittance spectrum of a ZrO₂ sample (no additional oxygen during deposition) together with a theoretical curve obtained by fitting of the parameters of a dielectric model to the experimental data. A relatively bad fit is shown to demonstrate the difficulties of the simple one-layer model.

ready successfully applied for In₂O₃:Sn films.[6,7] The model for the isolating films investigated here comprises a single harmonic oscillator to account for the interband transitions and a term that represents the optical transitions close to the band edge.[8] For the degenerate semiconductor In₂O₃:Sn, a third term that represents the intraband transitions that are due to free electrons had to be added that is not needed here.

For every deposition performed, there are two samples. Together with the two evaluation methods we get four data points for every deposition and can estimate the experimental error.

3. Results and Discussion

A. Refractive Index and Mass Density

Figure 1 shows a transmittance spectrum together with a simulated spectrum obtained by dielectric modeling. We have chosen an example with a relatively bad fit to show the potential error sources of this method: The minima are not exactly fitted and the interference maxima are smaller, because the experimental curve exceeds the transmittance of the substrate. The reason for the existence of these sources of error is that the film is optically not homogeneous.[9] It is in principle possible to model the film as a multilayer to account for an index profile. However, we did not apply this method because it adds more adjustable parameters to the model that cannot be checked by independent measurements. The evaluation of the extrema according to Eqs. (1) and (2) is usually straightforward except for the spectra of SiO₂ on quartz.

We have investigated the materials used in our optical workshop for optical coatings: MgF₂, SiO₂, Al₂O₃, ZrO₂, HfO₂, and TiO₂. Comparing the film thicknesses determined from the optical spectra with those obtained by profilometry, we found that there is a constant absolute deviation of ±10 nm, indepen-

Table 1. Range of Density and Refractive Index of Our Films

Material	ρ (g/cm^3)	n (at 550 nm)	$n = n_0 + m\rho$
SiO$_2$	1.4–2.1	1.43–1.49	1.32(3) + 0.075(5)ρ
ZrO$_2$	3.6–4.7	1.75–2.02	1.05(6) + 0.21(2)ρ
HfO$_2$	6.6–7.9	1.85–1.98	1.27(3) + 0.088(4)ρ

dently of the sample thickness. The coincidence is good down to thicknesses of ~200 nm and even to 150 nm for materials with a high n. This shows that the range of validity of the Swanepoel method extends to film thicknesses smaller than supposed in the literature. In Ref. 10 it is stated that the Swanepoel method can be applied for an optical thickness bigger than 0.6 μm, a value that is roughly twice our lower limit. Direct evaluation of the interference minima gives thicknesses that are often closer to the geometrical thicknesses than those obtained from dielectric modeling. The reason is that the simulated curve is fitted to the whole transmittance curve and may slightly miss the exact positions of the minima, whereas the information for the film thickness is

Table 2. Literature Data for Compact Materials

Material	ρ (g/cm^3)	n	λ (nm)	Reference
SiO$_2$				
Fused quartz	2.2	1.460	546	11
Crystal quartz	2.653	1.546, 1.555	546	12
	2.65	1.544, 1.553	589	13
Cristobalite	2.32	1.487, 1.484	589.3	14
ZrO$_2$				
Monoclinic	5.68	2.176	?	15
Baddeleyite	5.7	2.13, 2.19, 2.20	?	16
HfO$_2$				
Monoclinic	10.14	?		17
Cubic	?	2.125	550 nm	18

mainly in the position of the interference minima ($n_1 > n_2 > n_3$) or maxima ($n_1 < n_2 > n_3$).

The refractive indices obtained with the two methods coincide within 1%. The values obtained from the computer simulation are often slightly smaller than those obtained by means of Eq. (1). The reason is that in the simple computer model the transmittance of the interference maxima is forced to be that of the substrate, whereas in reality it may be lower because of scattering of film inhomogeneities or higher because of unintentional double layering (antireflection effect); see Fig. 1.

Our investigation of evaporated TiO$_2$ films has already been published.[1] We now investigate SiO$_2$, ZrO$_2$, and HfO$_2$ in more detail. The ranges of mass density ρ and of refractive index n at λ = 550 nm obtained for these materials in our experiments are summarized in Table 1. Some literature data for compact materials are given in Table 2.[11–18]

In Fig. 2 the packing density of the films is plotted versus the oxygen pressure during deposition. The density decreases with increasing pressure, similar to our observation of TiO$_2$.[1] The reason is increasing scattering of the evaporated species, leading to thermalization of their energies and randomization of their flight directions. This results in less perfect film growth with a higher pore volume. Similar results were reported in the literature for HfO$_2$ films: packing densities of 0.80 for $p_{O_2} = 4 \times 10^{-4}$ and of 0.64 for 10^{-3} (1 bar = 100 kPa).[19]

The surface roughness of films with relatively low and high densities, together with the grain sizes obtained from atomic force micrographs, are listed in Table 3. There is no general correlation among density, grain size, and roughness. For ZrO$_2$ the roughness is the same for all films. For SiO$_2$ the roughness of low-density films is relatively greater. The reason is the existence of protruding grain boundaries. Such films exhibit square grains, whereas high-density films are composed of grains of various shapes. For
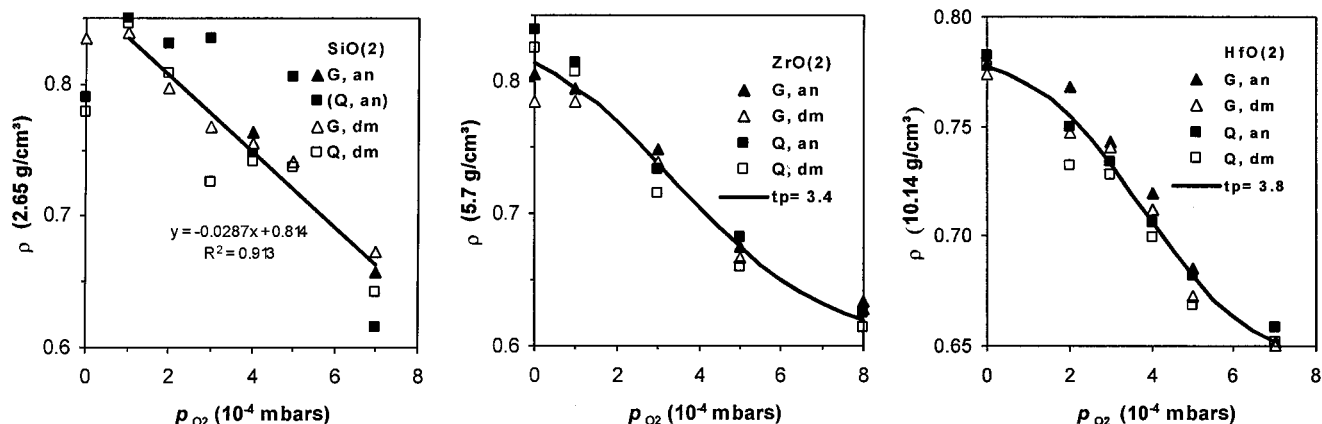

Fig. 2. Packing density of the films as a function of the oxygen pressure p_{O_2} during deposition. The data for ZrO$_2$ and HfO$_2$ are fitted with a *tangens hyperbolicus*, the turning point of which is given in each figure. The data (Q, an) for SiO$_2$ are excluded from the linear fit. G and Q mean glass and quartz substrates, respectively; an and dm mean evaluation of the film thickness by the analytical method and by dielectric modeling, respectively. R^2 is the correlation coefficient of the fit to the experimental data; t_p denotes the turning point of the *tangens hyperbolicus* function used for the fit.

Table 3. Evaluation of Atomic-Force Micrographs of Films with Relatively Low and High Packing Densities

Material (Temperature)	Packing Density	Roughness (nm)	Grain Size (nm)
SiO$_2$ (300 °C)	0.61	2.9	80
	0.80	1.3	20
HfO$_2$ (300 °C)	0.65	1.3	100
	0.78	3.3	50
ZrO$_2$ (300 °C)	0.64	2.7	100
	0.82	2.7	150
ZrO$_2$ (170 °C)	0.61	2.0	30
	0.79	2.0	120

HfO$_2$ the roughness of high-density films is relatively greater.

Deposition without additional oxygen is generally possible. To get better reproducibility it is, however, better to apply a defined oxygen pressure of ~3 × 10^{-4} mbars. The refractive index n at λ = 550 nm is an approximately linear function of the
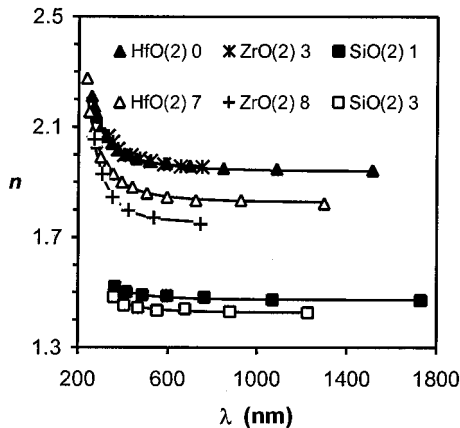

Fig. 3. Some representative dispersion curves: SiO$_2$, deposited at $p_{O_2} = 1 \times 10^{-4}$ and 3×10^{-4} mbars; ZrO$_2$ (3; 8×10^{-4} mbars), and HfO$_2$ (0; 7×10^{-4} mbars).

film density. The corresponding formulas are given in Table 1.

B. Dispersion Curves

Figure 3 shows some representative dispersion curves obtained by means of Eqs. (1) and (2). All are well represented by the Cauchy formula

$$n(\lambda) = A + \frac{B}{\lambda_2} + \frac{C}{\lambda_4} \qquad (4)$$

represented by the curves in Fig. 3.

The fit of parameters A, B, and C to the experimental data was obtained by multilinear regression. B and C show a large scatter and are not correlated with the density. They may be set to the average value for all samples. Furthermore, B may be set to zero for SiO$_2$ without changing the dispersion curves visibly. The values for A are shown in Fig. 4, together with the experimental values for n at 550 nm. Their supposed functional dependence on density is also given in Fig. 4.

The bandgaps of the materials, as obtained from dielectric modeling, are as follows: E_g = 5.25 eV for ZrO$_2$ and 5.7 eV for HfO$_2$, independently of the preparation conditions. In the literature, bandgaps of E_g = 5.5–5.6 eV have been reported for HfO$_2$.[20] No reliable data can be obtained for SiO$_2$ because the bandgap (E_g < 180 nm) is beyond the measured spectral range. The sharpness of the band edge was modeled in the computer simulation by an exponential function. The characteristic energy of this exponential function is ~0.2 eV for low-density HfO$_2$ and ZrO$_2$ and increases with the density.

The Sellmeier formula

$$n(\lambda) = \left(1 + \frac{a}{1 + b/\lambda^2}\right)^{1/2} \qquad (5)$$

contains only two free parameters and is, therefore, often preferred for the design of optical coatings. Our data may also be represented by Eq. (5), although
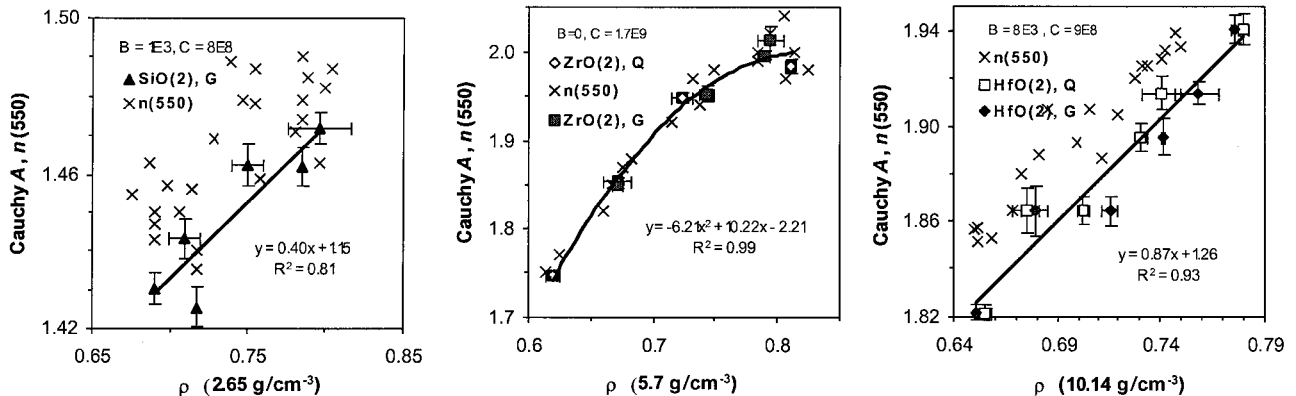

Fig. 4. Refractive-index parameters versus packing density of the thin films. G and Q mean glass and quartz substrates, respectively. R^2 is the correlation coefficient of the linear fit to the data. Crosses refer to the experimental refractive index at λ = 550 nm. The filled and open symbols represent parameter A of the Cauchy formula, Eq. (4), for films on quartz and glass, respectively.

with less accuracy in the region where the wavelength approaches the bandgap. The data are not highly sensitive to b, so a constant value may be taken for all curves of a material. Parameter a depends on the film density:

$$a_Z = -0.60 + 0.73 \, [\text{cm}^3/g]\rho,$$

$$b_Z = -0.25 \times 10^5 \, \text{nm}^2 \qquad (\text{ZrO}_2),$$

$$a_S = 0.23 + 0.43 \, [\text{cm}^3/g]\rho,$$

$$b_S = -0.15 \times 10^5 \, \text{nm}^2 \qquad (\text{SiO}_2),$$

$$a_H = 0.30 + 0.30 \, [\text{cm}^3/g]\rho,$$

$$b_H = -0.22 \times 10^5 \, \text{nm}^2 \qquad (\text{HfO}_2). \qquad (6)$$

Equations (4) and (5) are valid in the range where the extinction is negligible. This is no restriction for our purpose because coatings for laser optical components are useful only for vanishing extinction.

The variation in the index of ZrO_2 with the packing density of the films is so large that it is possible to produce dielectric mirrors just by changing the oxygen pressure during deposition. E.g., a mirror with 100% reflection at 770–830 nm may be obtained with 81 layers (low index, $a_z = 1.98$; high index, $a_z = 2.92$).

Our values for the refractive indices are comparable to those reported in the literature.

For ZrO_2 prepared by electron-beam evaporation at various particle incidence angles, $n(600 \, \text{nm}) = 1.975$ (at 0° particle incidence) to 1.68 (at 75°) was found.[21] For our films, values of 2.02–1.76 were found for this wavelength, depending on the density. These two findings are consistent because it is well known that at oblique incidence the film density decreases. The values for crystalline ZrO_2 are 2.176 and 2.16 for the ordinary and the extraordinary beams, respectively.[16]

For SiO_2 thin films the values of $n(550 \, \text{nm})$ range from 1.42 to 1.53, with the lowest and highest values obtained for solgel deposition and ion-assisted deposition, respectively.[14] For reactively evaporated films, values of ~ 1.47 were reported that are comparable to our results.

For HfO_2, values of $n(550 \, \text{nm}) = 1.92$–2.12 were reported. The higher value was obtained for films prepared in conditions of Xe^+-ion-assisted evaporation.[22] At $\lambda = 308 \, \text{nm}$, values of n from 2.01 to 2.15 were reported.[23] The films were prepared by electron-beam evaporation, and the higher n values were obtained for ion-beam-assisted deposition, for which higher packing densities were expected. Our values at this wavelength ranged from 1.98 to 2.07. Evaporation assisted by 50-eV Xe^+ bombardment yielded films with $n(550 \, \text{nm}) = 2.04$.[24] The refractive index depends also on the base pressure before the intake of O_2:$n(550 \, \text{nm}) = 1.99$ for $p = 13 \times 10^{-4} \, \text{Pa}$ and

$n(550 \, \text{nm}) = 2.03$ at $5 \times 10^{-4} \, \text{Pa}$, for a substrate temperature of 250 °C.

Reference 25 reports dispersion curves for HfO_2 films prepared by plasma ion-assisted deposition and ion plating. Both curves lie above our curves shown in Fig. 3. This is to be expected because it is known that these deposition methods produce denser films than reactive evaporation.

The Sellmeier formula with the parameters as given above was used to design layer stacks with a commercial program.[26] The agreement between predicted and obtained optical properties was good for stacks of 2–80 layers.

C. Refractivity models

In the literature on optical materials, n and ρ data are often represented as Lorentz–Lorenz plots of $(n^2 - 1)/(n^2 + 2)$ versus ρ, and molecular polarizability is inferred from the slope of a straight line fitted to the data. However, such an interpretation is valid only for a homogeneous distribution of point dipoles, a situation found, e.g., in gases. In solid materials the straight lines yield nonzero ordinate intercepts, unlike in the Lorentz-Lorenz model.[1]

The Lorentz–Lorenz relation ignores two effects that are important for thin solid films: the atomic orbitals may overlap, and the film contains pores. These effects are dealt with by a general refractivity formula and an effective-medium approach, respectively.

1. General Refractivity Formula

In the classic theory of dielectrics, the atoms are considered ideal point dipoles and the local field at the site of an atom is given by the Lorentz expression

$$E_{\text{loc}} = E + \frac{1}{3\varepsilon_0} P \qquad (\text{SI}). \qquad (7)$$

For materials with covalent bonding an overlap of neighboring orbitals has to be taken into account by an additional field represented by a term γ:

$$E_{\text{loc}} = E + \frac{1}{\varepsilon_0}\left(\frac{1}{3} - \frac{\gamma}{4\pi}\right)P$$

$$= E + \frac{1}{\varepsilon_0}\left(\frac{b}{4\pi}\right)P \quad (\text{SI}). \qquad (8)$$

The factor 4π in Eq. (8) is introduced to get the same numerical values for b as in Ref. 27, in which the cgs system of units is used. The general refractivity formula is then given by

$$\frac{n^2 - 1}{n^2 + [(4\pi/b) - 1]} = \left(\frac{b}{4\pi}\right)\frac{1}{\varepsilon_0}\rho\left(\frac{\alpha}{M}\right) \quad (\text{SI}), \qquad (9)$$

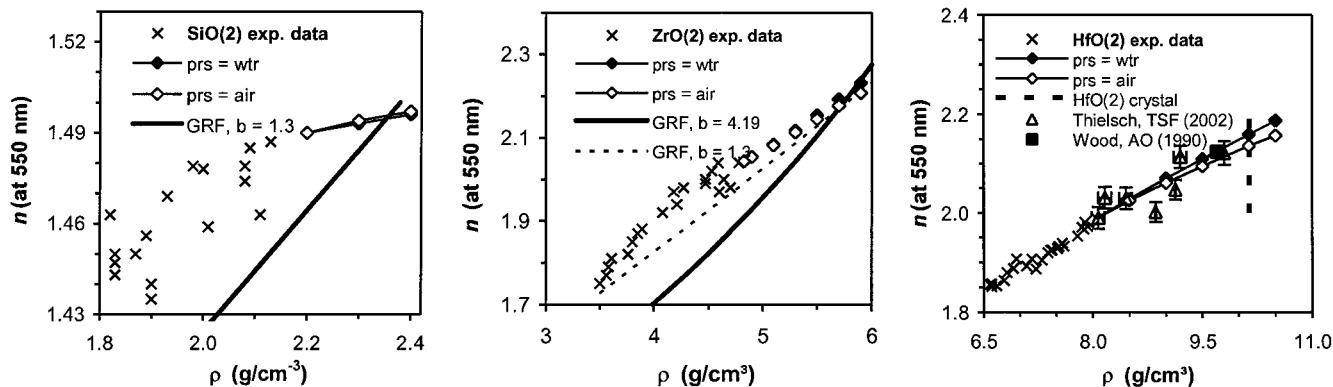which reduces to the well-known Lorentz–Lorenz relation for $b = 4\pi/3$ equivalent to $\gamma = 0$.

Fig. 5. Correlation of n (at 550 nm) and ρ. Crosses represent the experimental data; diamonds represent potential values for compact amorphous grains consistent with the Bruggeman relation. The pores are assumed to be filled with air or with water. Solid curves represent the general refractivity formula (GRF), Eq. (9).

Equation (9) was used for a regression analysis of the (n, ρ) data of various isochemical series of densified silica glasses and yielded $(\alpha/M) = 0.037$ and $b = 1.30(2)$.[27]

The function $n = n(\rho)$ derived from Eq. (9) and $b = 1.3$ is represented in Fig. 5 (SiO$_2$) by the thick solid curve. For ZrO$_2$ we know ρ and n values only for the monoclinic crystalline form. The hypothetical curves for $b = 4\pi/3$ and $b = 1.3$ are represented in Fig. 5 (ZrO$_2$) by the thick solid curve and the dotted curve, respectively.

2. Effective-Medium Approach

The density variation of thin films is due mainly to different pore volumes, and the data have to be interpreted by means of effective-medium theories. Such an approach, based on the Bruggeman formula, was applied to TiO$_2$ films of various densities.[28] The basic hypothesis is that all films of a series are built with the same type of grain and the variation in the density of the films is due to different packing densities. Several values of bulk grain density ρ_b were tried hypothetically. The pores may be empty or filled with water. For every hypothesis, refractive index n_b of the respective grain is determined by a fit to the experimental data of the whole sample series.

This procedure has now been applied to the data of SiO$_2$, ZrO$_2$, and HfO$_2$. The results are represented in Fig. 5 by diamonds. Open and filled symbols refer to pores filled with air or with water, respectively. This distinction is relevant only for SiO$_2$. The difference for ZrO$_2$ and HfO$_2$ is less than 1%.

Of the many potential (ρ_b, n_b) pairs, physically meaningful ones have to be selected. We have chosen the value at the intersection with the general refractivity lines that represent bulk materials with homogeneously distributed dipoles and with the packing density proportional to the dipole density. As the geometric form of the pores is not known, the results of our effective-medium approach should be interpreted with caution and be taken as a first estimate.

The bulk grains of SiO$_2$ and ZrO$_2$ are close to the points for crystalline quartz and the monoclinic form

of ZrO$_2$. It was observed earlier that the values for $n(550 \text{ nm})$ are bigger than the respective refractive indices of amorphous bulk silica materials.[14] Refractive indices of amorphous films deposited with ion-beam assistance are even close to the value of crystalline quartz. We explain this with the microstructure with compact amorphous grains suggested above.

Thielsch et al. reported the correlation of the refractive index at 550 nm with the packing density of HfO$_2$ layers deposited by different techniques (e.g., ion-assisted evaporation).[29] Their data have been incorporated into Fig. 5 (HfO$_2$). Also incorporated into Fig. 5 is the value for n reported for a single crystal.[18] As the density of this crystal was not reported, we take the value 9.7 g/cm^2 assumed in Ref. 29. All these data scatter about our theoretical curve. We have also plotted a vertical line at $\rho_b = 10.13 \ g/cm^3$ (inferred from the lattice constant; see Table 2). A hypothetical compact grain with this density has $n_b = 2.13$. Some authors report the occurrence of a (200) x-ray reflex of monoclinic HfO$_2$ in films deposited by electron-beam evaporation at a substrate temperature of 200 °C.[30] Therefore it seems plausible that a phase with nearly crystalline density is created in our films that are deposited at 300 °C.

4. Conclusions

It is possible to derive the thicknesses and the refractive indices of thin nonabsorbing films on transparent plates from transmittance spectra by means of simple analytical formulas. These thicknesses are reliable down to 150 nm and are comparable with the geometrical thickness measured with a stylus profilometer. The refractive indices are similar to those obtained by dielectric modeling, i.e., fitting calculated spectra based on physical models to the experimental data.

We determined the mass of the films by weighing. The packing density of reactively evaporated SiO$_2$, ZrO$_2$, and HfO$_2$ thin films varies from 0.82 to 0.6, depending on the pressure during deposition (as

much as 8×10^{-4} mbars). It decreases with increasing pressure.

The dispersion curves of the films are well represented by the Cauchy formula. Parameter A, which represents the wavelength-independent term, is a function that increases with the packing density. Parameters B and C, which represent the variation with $1/\lambda^2$ and $1/\lambda^4$, respectively, are constant for the respective materials. A reliable design of optical filters is also possible by use of the Sellmeier dispersion formula with density-dependent parameters.

The films can be modeled as a mixture of compact amorphous grains and empty pores. The (ρ, n) data are analyzed theoretically, based on a general refractivity formula that takes into account a homogeneous distribution of atoms with overlapping orbitals and the Bruggeman effective-medium theory. First estimates of density ρ_b and refractive index n_b of the bulk grains consistent with this approach correspond to the values of crystalline SiO_2 (quartz) and ZrO_2 (monoclinic), respectively. If we assume that the bulk HfO_2 grains have the crystalline density derived from the lattice constant, their refractive index is estimated to be $n_b = 2.13$.

References and Notes

1. D. Mergel, D. Buschendorf, S. Eggert, R. Grammes, and B. Samset, "Density and refractive index of TiO_2 films prepared by reactive evaporation," Thin Solid Films **371,** 218–224 (2000).
2. Prof. Feierabend GmbH, Lise-Meitner-Allee 4, 44801 Bochum, Germany.
3. R. Swanepoel, "Determination of the thickness and optical constants of amorphous silicon," J. Phys. E. **16,** 1214–1222 (1983).
4. O. S. Heavens, *Optical Properties of Thin Solid Films* (Dover, New York, 1991), Sec. 6.2.
5. H. Ahrens, "Bestimmung der Absorptionsindices und der Struktur dielektrischer Aufdampfschichten in Abhängigkeit von den Herstellungsparametern," dissertation (Technische Universität Hannover, Hannover, Germany, 1974).
6. Scout 98 software. (M. Theiss, Hard- and Software for Optical Spectroscopy, Aachen, Germany; www.mtheiss.com).
7. D. Mergel and Z. Qiao, "Dielectric modelling of optical spectra of thin In_2O_3:Sn films," J. Phys. D **35,** 794–801 (2002).
8. S. K. O'Leary, S. R. Johnson, and P. K. Lim, "The relationship between the distribution of electronic states and the optical absorption spectrum of an amorphous semiconductor: an empirical analysis," J. Appl. Phys. **82,** 3334–3340 (1997).
9. O. Stenzel, *Das Dünnschichtspektrum. Ein Zugang von den Grundlagen zur Spezialliteratur* (Akademie-Verlag, Berlin, 1996).
10. Y. Laaziz, A. Bennouna, N. Chahboun, A. Outzourhit, and E. L. Ameziane, "Optical characterization of low optical thickness thin films from transmittance and reflectance measurements," Thin Solid Films **372,** 149–155 (2000).
11. D. R. Lide, ed., *CRC Handbook of Chemistry and Physics*, 76th ed. (CRC Press, Boca Raton, Fla., 1995–1996), p. 10–302.
12. *Silicium Teil B*, Gmelins Handbuch der Anorganischen Chemie, 8th ed. (Verlag-Chemie, Weinheim 1959), Part B, pp. 263 (n) and 321 (ρ).
13. Ref. 9, p. 4–137.
14. O. Anderson and C. Ottermann, "Properties and characterization of dielectric thin films," in *Thin Films on Glass*, H. Bach and D. Krause, eds. (Springer-Verlag, Berlin, 1997), pp. 165–167.
15. *Zirkonium*, Gmelins Handbuch der Anorganischen Chemie, 8th ed. (Verlag-Chemie, Weinheim 1958), pp. 232 (n) and 222 (ρ).
16. Ref. 11, p. 4–133.
17. J. Adam and M. D. Rogers, "The crystal structure of ZrO_2 and HfO_2," Acta Crystallogr. **12,** 951 (1959).
18. D. L. Wood, K. Nassau, T. Y. Kometai, and D. L. Nash, "Optical properties of cubic hafnia stabilized with yttria," Appl. Opt. **29,** 604–607 (1990).
19. B. André, L. Poupinet, and G. Ravel, "Evaporation and ion assisted deposition of HfO_2 coatings: some key points for high power laser applications," J. Vac. Sci. Technol. A **18,** 2372–2377 (2000).
20. S. Capone, G. Leo, R. Rella, P. Siciliano, L. Vasanelli, M. Alvisi, L. Mirenghi, and A. Rizzo, "Physical characterization of hafnium oxide thin films and their application as gas sensing devices," J. Vac. Sci. Technol. A **16,** 3564–3568 (1998).
21. M. Levichkova, V. Mankov, N. Starbov, D. Karashanova, B. Mednikarov, and K. Starbova, "Structure and properties of nanosized electron beam deposited zirconia thin films," Surf. Coat. Technol. **141,** 70–77 (2001).
22. M. Alvisi, S. Scaglione, S. Martelli, A. Rizzo, and L. Vasanelli, "Structural and optical modification in hafnium oxide thin films related to the momentum parameter transferred by ion beam assistance," Thin Solid Films **354,** 19–23 (1999).
23. M. Alvisi, M. di Giulio, S. G. Marrone, M. R. Perrone, M. L. Protopapa, A. Valentini, and L. Vasanelli, "HfO_2 films with high laser damage threshold," Thin Solid Films **358,** 250–258 (2000).
24. J. P. Lehan, Y. Mao, B. G. Bovard, and H. A. Macleod, "Optical and microstructural properties of hafnium dioxide thin films," Thin Solid Films **203,** 227–250 (1991).
25. P. Torchio, A. Gatto, M. Alvisi, G. Albrand, N. Kaiser, and C. Amra, "High reflectivity HfO_2/SiO_2 ultraviolet mirrors," Appl. Opt. **41,** 3256–3261 (2002).
26. Filmstar Software (FTG Software Associates, Princeton, N.J.; www.ftgsoftware.com).
27. J. Arndt and W. Hummel, "The general refractivity formula applied to densified silicate glasses," Phys. Chem. Miner. **15,** 363–369 (1988).
28. D. Mergel, "Modeling thin TiO_2 films of various densities as an effective optical medium," Thin Solid Films **397,** 216–222 (2001).
29. R. Thielsch, A. Gatto, J. Heber, and N. Kaiser, "A comparative study of the UV optical and structural properties of SiO_2, Al_2O_3, and HfO_2 single layers deposited by reactive evaporation, ion-assisted deposition and plasma ion-assisted deposition," Thin Solid Films **410,** 86–93 (2002).
30. D. Reicher, P. Black, and K. Jungling, "Defect formation in hafnium dioxide thin films," Appl. Opt. **39,** 1589–1599 (2000).